Caenorhabditis Elegans Segmentation Using Texture-Based Models for Motility Phenotyping

Ayala Greenblum, Raphael Sznitman, Pascal Fua, *Fellow, IEEE*, Paulo E. Arratia, and Josué Sznitman*

***Abstract*—With widening interests in using model organisms for reverse genetic approaches and biomimmetic microrobotics, motility phenotyping of the nematode *Caenorhabditis elegans* is expanding across a growing array of locomotive environments. One ongoing bottleneck lies in providing users with automatic nematode segmentations of *C. elegans* in image sequences featuring complex and dynamic visual cues, a first and necessary step prior to extracting motility phenotypes. Here, we propose to tackle such automatic segmentation challenges by introducing a novel texture factor model (TFM). Our approach revolves around the use of combined intensity- and texture-based features integrated within a probabilistic framework. This strategy first provides a coarse nematode segmentation from which a Markov random field model is used to refine the segmentation by inferring pixels belonging to the nematode using an approximate inference technique. Finally, informative priors can then be estimated and integrated in our framework to provide coherent segmentations across image sequences. We validate our TFM method across a wide range of motility environments. Not only does TFM assure comparative performances to existing segmentation methods on traditional environments featuring static backgrounds, it importantly provides state-of-the-art *C. elegans* segmentations for dynamic environments such as the recently introduced wet granular media. We show how such segmentations may be used to compute nematode "skeletons" from which motility phenotypes can then be extracted. Overall, our TFM method provides users with a tangible solution to tackle the growing needs of *C. elegans* segmentation in challenging motility environments.**

***Index Terms*—*Caenorhabditis elegans*, computer vision, model organism, motility, phenotyping, segmentation.**

I. Introduction

DUE to its short life cycle [1], knowledge of its complete cell lineage [2], [3], the simplicity of its nervous system [4], and a fully sequenced genome [5], the nematode *Caenorhabditis elegans* has become a ubiquitous model organism to investigate the genetics of development, neuroscience, and behavior. An active area of research lies in behavioral motility phenotyping for reverse genetic approaches, where specific genes of interest are identified from whole-genome sequences [6].

Motility phenotyping of *C. elegans* generally aims at quantifying locomotive traits of individual (or groups of) nematodes, including but not limited to speed [7], [8], wavelength, and frequency of body undulations [9], [10], body curvature [11], [12], and posture reversals known as "omega turns" [13]. Most recently, nematode tissues properties have been estimated from imaged nematode body postures [14]–[18] as well as locomotive propulsive forces [19]–[23]. Alternatively, nematode imaging has been used to reconstruct basic body postures, known as "eigenworms" [24], [25], to define behavioral motifs that allow clustering of mutants into related groups [26].

Unfortunately, linking locomotion phenotypes to genotypes remains a cumbersome and time-consuming task. It requires first imaging numerous assays of nematodes and then carefully annotating hundreds, if not thousands, of nematodes from image sequences. Traditionally, this latter point has often been performed manually, imposing a labor-intensive and error-prone process. To alleviate the burden of annotating large image sets, automated analysis tools based on computer vision and machine learning techniques have emerged in view of designing high-throughput behavioral assays [6], [28], [30], [31], including drug screening applications [32]–[34]. In effect, they provide a roadmap for a systematic, reliable, and (semi-) automatic extraction of key phenotypic attributes.

Automated behavioral analysis tools almost unanimously require first extracting *C. elegans* postures from binary images, or *segmentations*, so as to separate the nematode from its environment (*background*). This segmentation process has been tackled using simple image intensity thresholds [8], [10], [12], [35]–[37], adaptive intensity thresholds [11], [13], [38], and more sophisticated statistical models [39], [40]. Central to all these methods is their complete reliance on nematode and background raw image intensities to guide the segmentation process. While these methods have been shown to be effective for automatic segmentation across a range of motility environments, such as locomotion on substrates [41]–[44] [see Fig. 1(a)], in fluids [19], [27], [43], [45], [46] [see Fig. 1(b)], or in patterned maze environments [28], [47]–[55] [see Fig. 1(c)], they are ill-suited, if not entirely compromised, when dealing with more challenging backgrounds that contain complex textures and/or are dynamic [e.g., Fig. 1(d)], where the background appearance changes significantly as the nematode moves within the surrounding medium [29], [56]. In particular, these complex

Manuscript received July 28, 2013; revised November 28, 2013; accepted January 2, 2014. Date of publication January 9, 2014; date of current version July 15, 2014. This work was supported in part by the European Commission (FP7 Program) through a Career Integration Grant PCIG09-GA-2011-293604 and a US–Israel Binational Science Foundation Grant BSF Nr. 2011323. The work of Dr. Raphael Sznitman was supported in part by the European Commission (FP7 Program) through an ERC Grant MicroNano. A. Greenblum and R. Sznitman are first co-authors. *Asterisk indicates corresponding author*

A. Greenblum is with the Department of Biomedical Engineering, Technion—Israel Institute of Technology, 32000 Haifa, Israel (e-mail: ayalag@tx.technion.ac.il).

R. Sznitman and P. Fua are at the Computer Vision Laboratory, École Polytechnique Fédérale de Lausanne, 1015 Lausanne, Switzerland (e-mail: raphael.sznitman@epfl.ch; pascal.fua@epfl.ch).

P. E. Arratia is with the Department of Mechanical Engineering and Applied Mechanics, University of Pennsylvania, Philadelphia, PA 19104 USA (e-mail: parratia@seas.upenn.edu).

*J. Sznitman is with the Department of Biomedical Engineering, Technion—Israel Institute of Technology, 32000 Haifa, Israel (e-mail: sznitman@bm.technion.ac.il).

Color versions of one or more of the figures in this paper are available online at http://ieeexplore.ieee.org.

Digital Object Identifier 10.1109/TBME.2014.2298612

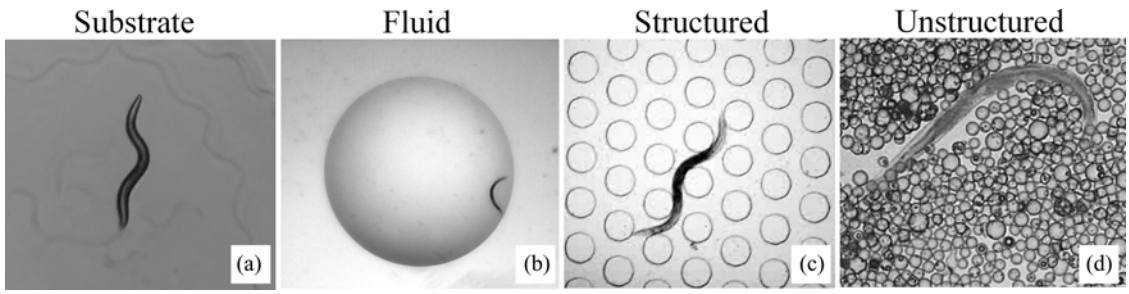

Fig. 1. Sample selection of environments for *C. elegans*' motility assays. (a) Nematode crawling on an agar substrate (gene: *dat*-1, strain: *RM*2702, allele: *ok*157, chromosome: *III* genotype: *dat*-1(*ok*157)*III*; see supplementary video in Brown *et al.* [6]). (b) Nematode swimming in an aqueous drop of M9 buffer solution (see example in Ghosh and Sznitman [27]). (c) Nematode locomoting through a structured microfluidic maze of pillars (source: nmeth.1630-S2.avi, see supplementary video in Albrecht and Bargmann [28]). (d) Nematode locomoting through an unstructured domain made of polydisperse granular media (source: supplementary material in Juarez *et al.* [29]). *C. elegans* shown in examples (a)–(d) are all approximately 1-mm long and illustrate environments with variations in lighting conditions, spatial resolution, field of view scale, and background complexity.

environments are increasingly relevant in view of designing artificial biomimmetic microrobots [57]–[59].

It is in this latter context [i.e., Fig. 1(d)] that we propose a novel statistical strategy for semisupervised segmentation of *C. elegans*. In order to initialize our algorithm, only a single image is required to be manually annotated by a user. Our method first learns a number of distinct image features that capture texture and intensity information regarding the nematode and the background, respectively. From the user-provided segmented image, we determine those features that are informative and then segment pixel-by-pixel each image of a sequence by using a probabilistic classification model and the learned features. We show experimentally that our method provides comparable, if not improved, segmentation results for traditional environments relative to intensity-based methods. Most importantly, our method delivers for the first time usable phenotypic results in challenging granular environments where state-of-the-art methods fail entirely.

Below, we begin by describing previous related works. In Section III, we present our method in detail and outline both the model assumptions and dependencies on the end-user. Next, we present in Section IV in-depth experiments evaluating our method and compare performances to existing state-of-the-art methods. In Section V, we briefly illustrate how such nematode segmentations are typically utilized to extract motility phenotypes, and conclude with some remarks in Section VI.

II. Related Work

While a growing body of work on segmentation techniques has surfaced in the last decade in the computer vision and machine learning communities, methods adapted for the specific needs of nematode segmentation still remain somewhat scarce. One bottleneck lies in the ongoing scarcity of extensive, open-access datasets of annotated nematodes; these are pivotal in using segmentation methods that rely on statistical learning [6], [60], [61].

When considering nematode segmentation with little training data, i.e., a handful of labeled images, the most widespread approach relies on a simple intensity-based threshold at any given pixel location [8], [10], [12], [35]–[37], where a user manually selects an appropriate range of intensities characterizing the imaged nematode. A variation to this approach has been suggested with the use of an adaptive threshold, where nematode intensities or *appearance*, are assumed to significantly differ from the mean background intensities [11], [13], [38]. One intrinsic drawback with intensity-based thresholds lies in their limited versatility across the growing selection of nematode motility environments [40] and have thus been traditionally limited to crawling assays on substrates [41]–[44] [see Fig. 1(a)]. The overarching bottleneck with intensity-based thresholding remains that accurate segmentations require a significant effort on the user-end to select appropriate threshold values along with other noise canceling schemes (e.g., median filters, morphological operators, background subtraction, etc.). These limiting factors ultimately jeopardize the efficiency of such strategies for motility assays across diverse environments [see Fig. 1(b)–(d)], and thus still impose a heavy burden on the user.

To overcome some of these limitations, statistical learning techniques have been recently applied to nematode segmentation [62], [63], where the strategy lies in systematically learning how background intensity pixels are distributed. Here, the learning process is done using a set of labeled images, or *training* images, to statistically model the background appearance by means of a mixture of Gaussians (MOG) model for each pixel, where the model parameters are estimated from the complete training set of images [39], [64], [65]. Unfortunately, the number of MOGs used corresponds to the total number of pixels in an image, and consequently, the number of parameters required becomes rapidly overwhelming. Hence, a large number of image frames are needed to estimate the MOG parameters accurately. Moreover, the entire background scene must be visible to estimate these parameters, since each image is used to model only the background and not the nematode. This latter condition is problematic when image sequences contain a nematode at all times, as is frequently the case in available data [17], [29], [43], [45], [50], [52].

More recently, Sznitman *et al.* [40] proposed to decompose the background into rectangular regions and learn a single MOG per region. This decomposition requires a far smaller number of MOGs to be learned compared to traditional background modeling techniques [39], leading to significantly reduced number

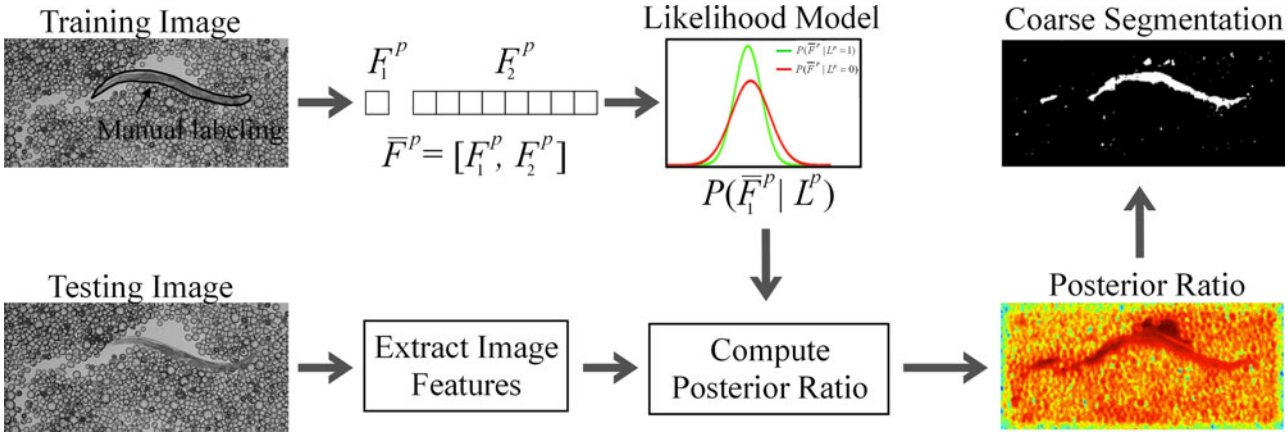

Fig. 2. Framework of the TFM. At training time, different features F_1^p and F_2^p for a given image pixel p are extracted from a single image with a manual segmentation of the nematode. The feature vectors are concatenated into one $\bar{F}^p$ and Gaussian likelihood models are then estimated (shown here in 1-D). At test time, $\bar{F}^p$ is then extracted at each pixel and the likelihood models are used to compute the posterior ratio (see text for details). The posterior ratio can be visually depicted at each pixel (heat map where green corresponds to small values and red to high values). To construct a coarse nematode segmentation, i.e., C^p for each pixel p, the posterior ratio is thresholded at a single value.

of training images required. The authors then use the likelihood of ratios to segment nematodes across various motility environments. While effective in a number of cases [40], the method yet fails when faced with complex, texture-rich scenarios; indeed, the central feature in the approach of [40] revolves around the local average pixel intensity and thus cannot disambiguate nematodes from background when both have similar intensities [e.g., Fig. 1(d)].

III. Method

Our goal is to provide users with nematode segmentations across image sequences. To make our method as practical and straightforward as possible for the end user, we restrict the amount of training data, i.e., the number of manually segmented nematodes, to be the first image in a sequence; namely, this restriction considerably alleviates the burden imposed on the expert user and delivers an attractive solution within the nematode community.

Our method will be broken into two parts: a coarse segmentation process and a second refinement stage. In the coarse segmentation stage, we use a single annotated image to compute a number of image texture features and learn those that are informative for a given particular image sequence. At test time, the informative features are treated as *factors* within a Bayesian model to infer which pixels belong to the nematode and which do not, providing first a coarse image segmentation. To provide smooth and consistent image segmentations, we perform the refinement stage which first uses the coarse segmentation as observations of a Markov random field (MRF) and then the mean-field variational inference technique [66] to compute the maximum posterior marginals (MPMs) of the pixel labels. To segment the resulting images in a sequence, we then evaluate informative priors from the computed MPMs, via Bayesian filtering, and provide coherent estimates to where the nematode is located across the image sequence. The details of our methods, which we refer to as the texture factor model (TFM), are described below.

TABLE I
Summary of Notation

$\mathcal{I} = (I_1, \ldots, I_T)$	Image sequence
S_t	Segmentation of image I_t
$\mathcal{D} = \{I_1, S_1\}$	Training set
L^p	Class label of pixel p
F_k^p	Feature vector k for pixel p.
$\bar{F}^p$	Feature concatenation vector for pixel p.
R^p	Ratio of class posterior probability of pixel p.
C^p	Coarse segmentation of pixel p.
θ	Sensitive threshold

A. Notation

Let I_t be the tth gray-scale image from an image sequence $\mathcal{I} = (I_1, \ldots, I_T)$. Each pixel p in an image is associated with a discrete class label, denoted $L^p \in \{0, 1\}$, indicating whether or not that pixel belongs to the nematode ($L^p = 1$) or the background ($L^p = 0$). In addition, we consider L^p to be a discrete random variable with probability distribution $P(L^p)$. We denote S_t as the segmentation image of I_t, where each pixel of S_t has value 0 or 1 corresponding to the class label of the associated pixel. We define our training data, $\mathcal{D} = \{I_1, S_1\}$, as the first image and segmentation from the image sequence $\mathcal{I}$, as depicted in Fig. 2. The remaining images of the image sequence are set to be our test data. As such, our goal is to infer $S_2, \ldots, S_T$ as accurately as possible. In order to determine if a pixel label belongs to the nematode or background, we will compute a set of $K \geq 1$ image features, denoted $F^p = \{F_1^p, \ldots, F_K^p\}$, where $F_k^p \in \mathbb{R}^{n_k}$ is a feature vector for pixel p; note that we also consider F_k^p to be a random vector. A summary of the notation used is presented in Table I.

B. Nematode Image Features and Model

In order to provide usable nematode segmentations across different experimental setups, we will introduce a number of image features. As with Ensemble Classifiers [67], this strategy allows good coverage of the positive/negative image statistics

and typically leads to robust segmentation [60]. In practice, we specify $K = 2$ defined as:

1) *Average Pixel:* we compute the feature $F_1^p \in \mathbb{R}$ as the average intensity value of a small window of 7×7 pixels centered on pixel p [8], [36], [37].
2) *RFS Feature:* we compute $F_2^p \in \mathbb{R}^{38}$ as the response of a set of 38 filters centered on pixel p. The filters used are the root filter set (RFS) that consists in a mixture of bar, Gaussian, and Laplacian of Gaussian filters with different parameters, respectively [68]. Historically, these have been shown to be effective in characterizing textured regions.

We describe in the following section how and when these features are used to segment nematodes.

C. Coarse Image Segmentation

We are interested in computing at each pixel p the posterior distribution of the class when a *subset* of image features, $\{F_m^p\}_{m=1}^M$, has been observed. This is written as

$$P(L^p = l|\{F_m^p\}_{k=1}^M) = \frac{1}{\mathcal{Z}} P(\{F_m^p\}_{m=1}^M|L = l)P(L^p = l). \tag{1}$$

In effect, (1) describes the probability that a pixel has label l when the features $F_1^p, \ldots, F_M^p$ have been observed for pixel p in the image. The equation has three multiplicative terms. First, the prior probability of the class label for a given pixel, $P(L^p = 1)$ which will be held at 1/2 to indicate an unbiased prior on the pixel label. Second, the normalization constant $\mathcal{Z} = P(F_1^p, \ldots, F_M^p)$ that can be expressed as

$$P\left(\{F_m^p\}_{k=1}^M\right) = \sum_{z=0}^{1} P(F_1^p, \ldots, F_M^p|L = z)P(L^p = z). \tag{2}$$

Third is the likelihood model $P(\{F_m^p\}_{m=1}^M|L = l)$ which describes the likelihood of feature scores when the underlying pixel is either part of the nematode or the background. While modeling this likelihood is challenging as it requires having sufficient data to characterize how each feature affects the others, we propose to simplify the likelihood by concatenating all the features together, $\bar{F}^p = [F_1^p, \ldots, F_M^p]$ and assuming

$$P(\bar{F}^p = f|L = l) = \begin{cases} \mathcal{G}(f; \mu_1, \Sigma_1), & \text{if } l = 1 \\ \mathcal{G}(f; \mu_0, \Sigma_0), & \text{if } l = 0, \end{cases} \tag{3}$$

where $(\mu_i, \Sigma_i), i = 0, 1$ are the parameters of a Gaussian distribution for when the pixel is part of the nematode and when it is not. In the following section, we describe how to estimate these parameters from the training image. Despite representing the likelihood model with (3) which is a strong assumption on the image dataset, we will show in our experiments that this assumption yet allows accurate segmentations of nematodes.

Given the above, for any test image, we can then compute a coarse estimate of whether or not a pixel belongs to the nematode or the background by calculating

$$C^p = \mathbb{1}_{\{R^p > \theta\}}, \tag{4}$$

where $\theta \in \mathbb{R}^+$ is a sensitivity threshold and where we define

$$R^p = \frac{P(L^p = 1|\{F_m^p\}_{k=1}^M)}{P(L^p = 0|\{F_m^p\}_{k=1}^M)} \tag{5}$$

as the ratio of posterior probability. As such, nematode pixels are those where the ratio of posterior probability is larger than the sensitivity threshold. In Fig. 2, we visually depict for a sample image the relation between R^p and C^p using a particular threshold value θ.

D. Feature Likelihood Models

To compute the likelihood models $P(\bar{F}^p|L), L = 0, 1$, we proceed in the following manner. For a given feature vector, $\bar{F}^p \in \mathbb{R}^n$, we must estimate the class conditional likelihood model, $P(\bar{F}^p|L = 1)$ and $P(\bar{F}^p|L = 0)$, which we consider to be Gaussian in nature. That is, $P(F_k^p|L = 0) \sim \mathcal{G}(F_k^p; \mu_k^0, \Sigma_k^0)$ and $P(F_k^p|L = 1) \sim \mathcal{G}(F_k^p; \mu_k^1, \Sigma_k^1)$, where $\mu_k^1, \mu_k^0 \in \mathbb{R}_k^n$ are mean vectors of dimension n_k and $\Sigma_k^1, \Sigma_k^0 \in \mathbb{R}^{n_k \times n_k}$ are covariance matrices of size $n_k \times n_k$.

To estimate the parameters $\mu_k^1, \mu_k^0, \Sigma_k^1, \Sigma_k^0$ for each feature, we make use of the user-provided training data available, $\mathcal{D} = \{I_1, S_1\}$. Using the image I_1 and its corresponding nematode segmentation S_1, we randomly sample 40% of the pixels that belong to the background and 40% of the pixels corresponding to the nematode nematode. At each of the sampled locations, we compute the feature set responses $F_1^p, \ldots, F_K^p$. We then use the maximum likelihood estimators [67] to estimate the parameters $\mu_k^1, \mu_k^0, \Sigma_k^1, \Sigma_k^0$ for each feature response.

E. Selecting Feature Subsets

While we have described a pool of image features, only a subset $\{F_m^p\}_{m=1}^M \in F^p$ of such features are effectively used in (5) when segmenting a particular image sequence.

To select this subset, we first estimate $P(\bar{F}^p|L = l), l = 0, 1$ using the training image I_1, for each possible combination of the image feature subsets. Then, we segment the same training image, using (5) and select the subset that segments best. Written more formally, we solve

$$\left\{\{F_m^p\}_{m=1}^M, \theta\right\} = \arg\max_{q \subset F^p, \theta} \mathcal{F}_1(\bar{C}_\theta^q, S_1) \tag{6}$$

where $\bar{C}_\theta^q$ is the coarse segmentation achieved using the feature subset q and sensitivity threshold θ, and $\mathcal{F}_1$ is the F-score segmentation accuracy measure [60] defined as

$$\mathcal{F}_1(\bar{C}_\theta^q, S_1) = 2 \cdot \frac{\text{precision} \times \text{recall}}{\text{precision} + \text{recall}}. \tag{7}$$

In effect, we evaluate each possible feature subset and sensitivity threshold to select the pair which maximizes the $\mathcal{F}_1$ accuracy measure. Both the subset and the threshold are then used to segment the rest of the image sequence $S_2, \ldots, S_T$.

F. Refined Segmentation

As noted earlier, the majority of previous automatic nematode segmentation algorithms perform some form of morphological operations during postprocessing so as to remove small errors in

segmentation. Here, rather, we attempt to rely on a more principled mechanism. In line with the probabilistic model introduced previously, we use the coarse segmentation results within an MRF.

For a given test image, we are interested in inferring the true segmentation S for all pixels p in that image. To this end, we use an MRF to describe the joint probability distribution of all pixel labels S and the coarse image segmentation C. We write the joint probability distribution for all pixels in the image as

$$P(C,S) = \frac{1}{Z}\prod_{p} P(C^p|S^p) \prod_{j\in\mathcal{N}_p} P(S^p S^j), \tag{8}$$

where $\mathcal{N}_p$ is a four-connected neighborhood of pixel p and Z is a normalizing constant. This model allows one to describe both the likelihood of a pixel label as well as its relation to neighboring pixels and has been shown to be effective in a number of related segmentation problems [60], [69]. Namely, this approach is particularly useful to encode smoothness and coherence.

Given the MRF model, we are interested in estimating the MPM, $P(S^p|C)$, which describes the probability of a pixel label, given the entire coarse image segmentation. Computing the MPMs can be achieved in a number of ways and we opt to do so with the well-established mean-field [66] approximation method. This method iteratively refines estimates of the MPMs and does so by first letting $P(S^p|C^p) = \mu_p = 0$ at initialization. Then, for $m = 1, \ldots, M$ iterations, we update the $P(S^p|C^p)$ by computing

$$\mu_{p+1} = \mu_p \alpha + (1-\alpha)\tanh\left(\sum_{j\in\mathcal{N}_p}\mu_j + \frac{1}{\beta}P(C^p|S^p)\right) \tag{9}$$

where α is a damping rate, $P(C^p|S^p) \propto (1+\exp(C^p))^{-1}$, and β is known as a so-called *temperature*. In our experiments, we set $\beta = 0.5$, iterate approximately $M = 100$ times, and let $\alpha = 0.5$. A detailed derivation of (9) can be found in [66].

Note that the strategy formulated in (9) is intended to smooth out incoherences that may have been produced during the coarse segmentation step. As such, the amount of smoothing necessary may be directly related to the relative size of the nematode in the image (i.e., proportion of pixels belonging to the nematode); this latter property is in part controlled by the MRF neighborhood size, i.e., 4-pixel neighborhood in the present framework. Hence, while the selected parameter may be appropriate in some cases, alternate values may be required for nematodes that appear larger.

G. Nematode Tracking

In the initial coarse segmentation, we assumed an unbiased prior, i.e., $P(L=1) = P(L=0) = 1/2$. We now show how an informative prior can be estimated for the purposes of nematode tracking throughout the remainder of the image sequences. In particular, when segmenting an image I_t at time step t, we will use the posterior distribution computed at the previous time step $t-1$ to estimate the new prior.

Specifically, we estimate the new prior over the entire image domain, $P(\hat{L}_t)$, by using traditional Bayesian filtering [70], defined as

$$P(\hat{L}_t) = \int P(L_t|L_{t-1})P(L_{t-1})dL_{t-1} \tag{10}$$

where $P(L_{t-1})$ corresponds to the posterior distribution computed for frame I^{t-1} using (1), and $P(L_t|L_{t-1})$ is a dynamics model which we assume to be Gaussian with mean zero and covariance Σ. In other words, we assume no change from one frame to the next, other than some intrinsic noise governed by Σ. In our experiments, we treat $\Sigma = 8I_2$, where I_2 is the identity matrix of size 2×2. As noted in the previous section, Σ can be modified to better model nematode motion across specific sequences [70]. In the remainder of this paper, we will use the term "Prior-TFM" to denote the use of informative priors, in contrast to the TFM.

IV. Experiments

In the following section, we provide both quantitative and qualitative performance results regarding our (Prior-)TFM method.[1] We do so by evaluating the TFM on real image sequences originating from motility assays in various environments. We compare our approach with existing methods to show and highlight the benefits of the TFM method.

A. Nematode Image Sequences

We evaluate our method across various motility environments. First, we make use of a number of representative backgrounds:[2] 1) crawling on an agar surface [see example in Fig. 1(a)], 2) swimming in an aqueous drop [see Fig. 1(b)], 3) swimming in gelatin-based solutions, and 4) navigating through microfluidic mazes constructed of micropillars [see Fig. 1(c)]. For each image sequence, approximately 35 manually labeled nematode segmentations are provided (see details in [40]).

In addition, we introduce two new image sequences featuring nematode locomotion in wet granular environments [29]. Briefly, the motility behavior of *C. elegans* is imaged in shallow channels filled with an aqueous buffer solution that contain either monodisperse or polydisperse particles set to a fixed packing fraction ϕ (i.e., ratio of volume of particles to total volume). Such environments are believed to mimic more accurately the soil-like milieus where *C. elegans* is found [29]. The first sequence contains polydisperse particles (52 ± 10-μm diameter, $\phi = 0.55$), while the second sequence contains monodisperse particles (60 ± 3-μm diameter, $\phi = 0.55$); 36 manually labeled frames are available for each sequence.

B. Evaluation

For each image sequence, we evaluated our method by training our TFM method on the first image and evaluating the remaining images in the corresponding sequence. We compare

[1] Source code and data will be made available online on the author webpage.

[2] Available for download at: http://sites.google.com/site/sznitr/code-and-datasets

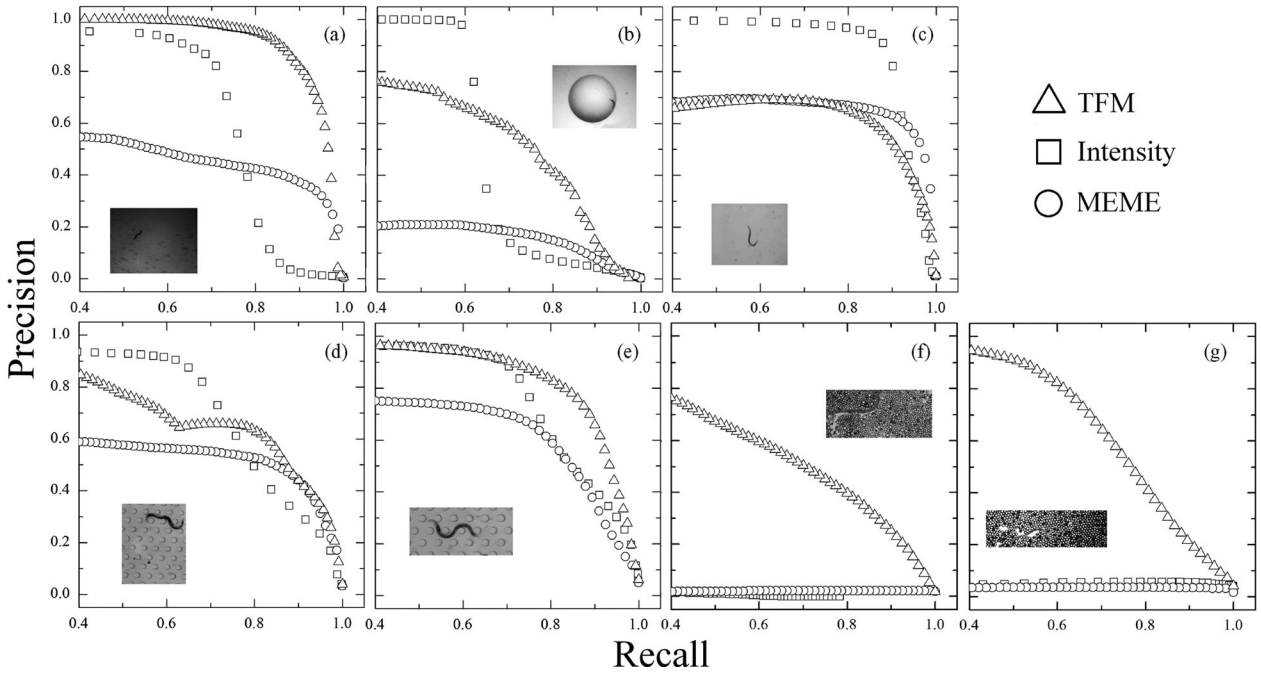

Fig. 3. PR curves for the coarse segmentation stage across selected motility environments: (a) crawling, (b) swimming in drops, (c) swimming in gelatin-based solutions (see supplementary material in Berri *et al.* [45]), (d) and (e) locomotion in microfluidic mazes (see supplementary material in Lockery *et al.* [50]), and (f) and (g) locomotion in wet granular media (see supplementary material in Juarez *et al.* [29]). For each image sequence, we depict the PR curve for the TFM, intensity-based, and MEME approaches, respectively. The TFM outperforms previous methods on the majority of sequences. In particular, the TFM provides substantial improvements for (f) polydisperse and (g) monodisperse environments.

our approach against a traditional intensity-based thresholding method [11], [13], the recent multienvironment model estimation (MEME) algorithm [40] and the segmentation strategy of Lucchi *et al.* [71]. In particular, this latter method extracts intensity histograms and co-occurrence features from *superpixels* to learn a radial basis function kernel support vector machine classifier. The classifier output is then used within an MRF to segment the object of interest. As with our TFM approach, this strategy also captures intensity and some amount of texture information, via the cooccurrence features. In each comparison method, we also only used the first image of the sequence to train the respective algorithms. Note that in contrast to traditional intensity-based thresholding and MEME, the method of Lucchi *et al.* has previously never been applied to nematode segmentation.

1) Coarse Segmentation: For the selected motility environments, Fig. 3 presents the precision recall (PR) curves obtained from each method. Any single point on a given curve corresponds to a potential segmentation threshold θ; curves that have both higher values of precision and recall are considered better, positioned nearer the top right corner of each plot, i.e., Precision = Recall = 1.

We see that for the image sequences shown in Fig. 3(a), (b), (f), and (g), the TFM outperforms all other methods. This is particularly true for the poly- [see Fig. 3(f)] and monodisperse environments [see Fig. 3(g)], where improvements are significant. In fact, both MEME and intensity methods are unable to characterize the nematode whatsoever, i.e., Precision ≈ 0. For the microfluidic environments [see Fig. 3(d) and (e)], all methods perform similarly, while for the drop scenario [see Fig. 3(b)], the intensity-based method exhibits only a slightly more advantageous PR curve.

To render the results of Fig. 3 more quantitative, we report in Table II the best F-score [as introduced in (7)] for each segmentation method applied. Namely, we show the best F-score obtained for each environment over the entire test set (see the first row in Table II) as well as on the single training image (see the second row in Table II). For the TFM method, we also show how different sets of features (i.e., Average pixel, RFS feature, and combination of both) perform on different environments. We notice that when determining with the TFM which feature sets to use from the first training image on an entire image sequence, our approach selects the best feature set possible barring the "Drop" image sequence. That is, evaluating each feature combination over the first training image and selecting the best one correlates rather well with the best feature set over the entire image sequence.

In general, we notice that either average pixel intensity or RFS combined with average pixel intensity performs best. This observation is reasonable as average intensity is a very strong visual cue for nematode segmentation [13], [40]. It appears that the TFM method augments in some instances this strong cue with more texture information such as in scenarios where environments are visually more complex (i.e., granular media).

When comparing the TFM against other methods, our approach outperforms significantly previous methods on the challenging poly- and monodispere environments. The best F-scores obtained with the TFM over the image stacks are $\sim$0.7 and 0.6, respectively. Comparatively, MEME and the intensity method both score below 0.1 for each image set. In general, these

TABLE II
SUMMARY TABLE OF BEST F-SCORES (7) FOR EACH SEGMENTATION METHOD AND CALCULATED FOR THE VARIOUS MOTILITY ENVIRONMENTS OF FIG. 3

	Method	Crawl ($n = 36$)	Drop ($n = 36$)	Gelatin ($n = 29$)	Microfl. I ($n = 37$)	Microfl. II ($n = 36$)	Polydisp. ($n = 36$)	Monodisp. ($n = 36$)
TFM	Avg.	**0.864** *0.889*	0.638 *0.681*	0.717 *0.885*	0.708 *0.663*	**0.816** *0.803*	0.158 *0.133*	0.053 *0.058*
TFM	RFS	0.556 *0.609*	0.310 *0.790*	0.443 *0.690*	0.462 *0.365*	0.601 *0.646*	0.600 *0.691*	0.492 *0.724*
TFM	Avg. & RFS	0.627 *0.678*	0.309 *0.822*	0.436 *0.708*	0.479 *0.386*	0.647 *0.690*	**0.697** *0.802*	**0.599** *0.798*
Others	Intensity	0.767 *0.767*	**0.739** *0.713*	**0.898** *0.913*	**0.747** *0.708*	0.784 *0.767*	0.071 *0.104*	0.035 *0.036*
Others	MEME	0.555 *0.451*	0.307 *0.320*	0.743 *0.659*	0.637 *0.562*	0.706 *0.572*	0.071 *0.074*	0.045 *0.046*

Shown are the best F-score obtained for the entire test set (first row) and on the single training image (second row). For TFM, the performance of different sets of features is also presented. For each environment, we highlight in bold the best F-best score obtained across all methods for the entire test set.

results indicate that the coarse segmentation produced by the TFM provides significant improvements for segmenting nematodes in unstructured environments such as wet granular media, where the background is both texture-rich and dynamic (i.e., particles are displaced as the nematode passes by). In other environments, the TFM performs similarly to the other methods, i.e., in some cases slightly better and in others slightly worse (see Table II). Below, we show how implementing the fine segmentation approach delivers state-of-the-art results on nematode segmentation across all environments.

2) Final Segmentation: To quantitatively evaluate and compare the final segmentation using the TFM, we depict in Fig. 4 both the nematode segmentation yield and the overall image segmentation error for the sequences tested in Fig. 3; these performance metrics have been recently defined [40] and are also reported here for the MEME, the intensity-based method, and the segmentation strategy of [71]. In addition, we also provide quantitative results for Prior-TFM, which uses temporal information as described in Section III-G.

We show for each evaluated image sequence in Fig. 4(a) the proportion of the nematode pixels that is correctly segmented in a given image (i.e., nematode yield). Correspondingly, we show in Fig. 4(b) the proportion of pixels that is incorrectly labeled over the entire image (i.e., surface error). In both plots, the results are produced from the best F-score obtained over the training set. While values of the nematode yield obtained from the TFM are generally similar to those for MEME and the intensity-based method applied across traditional environments [see Fig. 4(a)], the TFM achieves such results by maintaining a significantly smaller amount of labeling error over the rest of the image [see Fig. 4(b)]. This point is further highlighted when using Prior-TFM, where values of the nematode yield improve drastically for almost all image sequences, at the cost of a slightly higher surface error due to over segmentations.

Furthermore and importantly, both the MEME and intensity-based methods are simply unable to recover the nematode in the poly- and monodisperse environments, yielding high rates of nematode error. Both the TFM and Prior-TFM, on the other hand, maintain a reasonable surface error rate ($<2\%$) and produce nematode segmentations with a yield above 40% and 50% for the mono and polydisperse environments, respectively. In particular, the Prior-TFM approach delivers scores nearing or above the 80% mark, underlining the efficacy of implementing a nematode tracking technique.

When comparing segmentation results to the method of Lucchi *et al.*, both the TFM and Prior-TFM perform better across the array of traditional motility environments [see Fig. 4(a)]; yet, the segmentation approach of [71] appears more competitive for the mono and polydisperse environments where margins in nematode yield are much closer. In particular, Lucchi *et al.* performs similarly to Prior-TFM for the polydisperse sequence and only slightly worse for the monodisperse case.

In Fig. 5, we depict qualitative results of the final segmentation using the TFM and Prior-TFM on the poly- and monodisperse environments. For comparison, we also show the corresponding (human) manually labeled segmentations, i.e., groundtruth, as well as results produced with MEME and Lucchi *et al.* We immediately notice that MEME as well as the intensity-based method (not shown here) fail altogether in providing any reasonable segmentation of the nematode, further underlining the poor F-scores observed earlier in the PR curves (see Fig. 3 and Table II). In contrast, the TFM and Prior-TFM provide far more suitable segmentations, visually capturing the main characteristics of the nematode, i.e., shape and length. In the case of Lucchi *et al.*, the final segmentations on these two

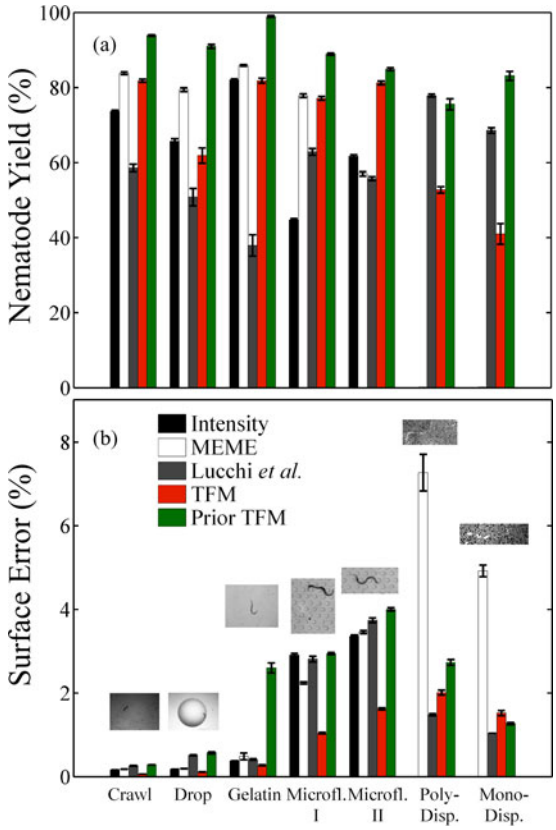

Fig. 4. Performance evaluation of final nematode segmentation. For the environments shown in Fig. 3, the TFM and correspondingly the Prior-TFM are compared to a traditional intensity-based thresholding approach [17], [18], as well as the recent methods of MEME [40] and Lucchi *et al.* [71]. (a) Nematode yield: proportion of the nematode region that is correctly segmented for a given image. (b) Surface error: proportion of pixels misclassified by a given algorithm over the entire image. For each environment shown, standard deviations (shown as error bars) are obtained across (manually-labeled) sequences of $n = 29$ to 37 images. Note that for the intensity-based method, successful segmentation are not available for both the mono- and polydisperse environments (see last two columns).

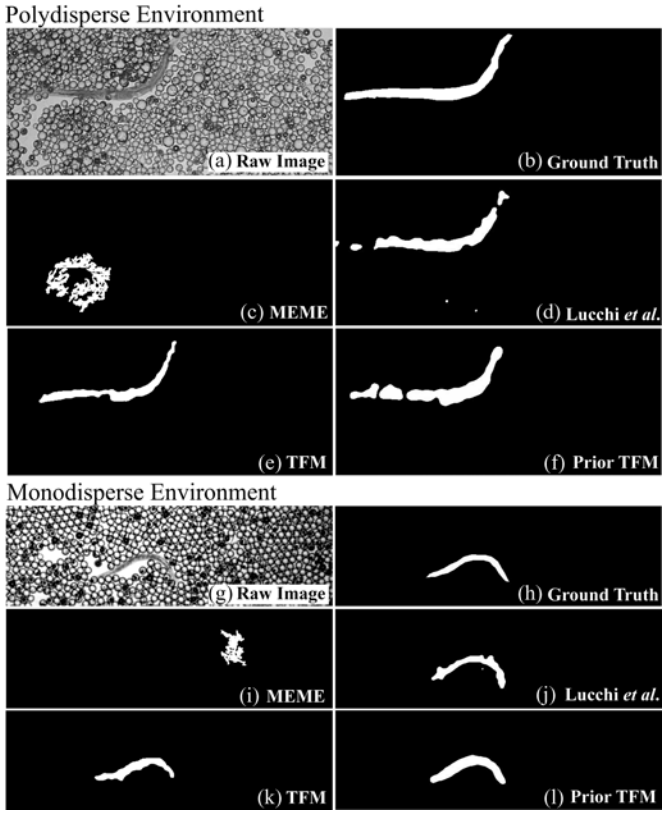

Fig. 5. Nematode segmentation in unstructured environments featuring poly- (a)–(d) and monodisperse (e)–(h) granular media; see supplementary material in Juarez *et al.* [29]). (a) and (e) Snapshots of raw images. Comparisons between nematode segmentations are, respectively, shown for 1) the ground truth (b) and (f), i.e., hand-segmented nematodes, 2) the MEME approach [40] (c) and (i), 3) the method of Lucchi *et al.* [71] (d) and (j), 4) the TFM shown in (e) and (k), and 5) the corresponding Prior TFM shown in (f) and (l).

challenging cases also capture the main characteristics of nematode but suffer from some jagged contours due to the superpixel preprocessing step.

Upon closer inspection, we notice that the TFM and Prior-TFM segmentations are far from perfect however. In fact, qualitative segmentation errors are apparent when particles are in the vicinity of the nematode or touching it. Portions of the nematode tail and head are also incorrectly segmented and lost. This latter problem has been previously noted and applies to a broader range of (static) backgrounds, including swimming and microfluidic environments [21], [40]. Namely, this problem occurs when the nematode extremities are transparent against the background. Finally, we note that for the polydisperse environment, the Prior-TFM delivers a disconnected nematode segmentation as is the case for the method of [71].

V. Discussion

From a user end, clean and reliable nematode segmentations represent the first and necessary step prior to extracting motility phenotypes of *C. elegans*. Indeed, the wide majority of quantitative motility traits characterizing *C. elegans* locomotion (e.g., speed, beating frequency, amplitude, body curvature, etc.) are not directly extracted from whole-body segmentations but rather from so-called "skeletons" that describe the nematode centerline data [10]–[12], [19], [41]. Here, we briefly discuss the feasibility of using nematode skeletons obtained with the TFM across complex environments such as wet granular media; to date, these latter environments have required tedious manual labeling to reliably extract usable skeletons [29].

In Fig. 6, tracking of nematode body postures are presented in both space and time; sample snapshots of the nematode moving through mono- [see Fig. 6(a)] and polydisperse [see Fig. 6(b)] wet granular media are shown with the corresponding body postures (i.e., skeletons). These skeletons are extracted using the method of [40], where nematode ends points are first extracted, and then a Bayesian marching algorithm is used to trace out the centerline between end points of the nematode using the image segmentation directly.

Changes in the motility behavior between the two environments can be qualitatively captured at a glance from the evolution of nematode skeletons over the image sequences. This is shown in Fig. 6(c) and (d) where the time evolution of skeletons is color-coded as a function of time; envelopes of body postures

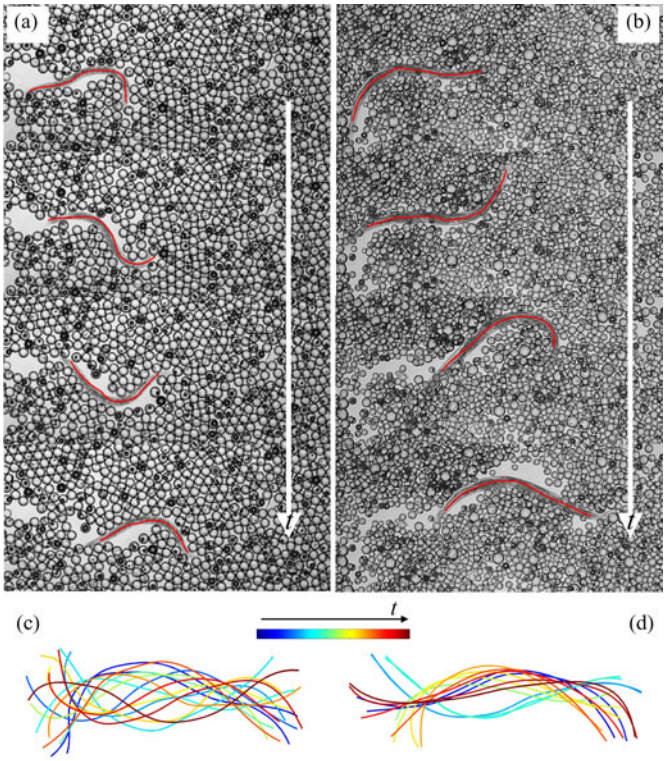

Fig. 6. Motility features using nematode skeletons. Micrographs of *C. elegans* moving through (a) mono- and (b) polydisperse wet granular media with a packing fraction of $\phi = 0.55$; raw image sequence available from supplementary material in [29]. For each snapshot, the corresponding nematode skeleton is superimposed (red) as obtained after final segmentation using the TFM and applying the skeletonizing algorithm of [40]. Corresponding color-coded temporal evolution of *C. elegans* skeletons over an image sequence for (c) mono- and (d) polydisperse media, respectively; skeleton lines are evenly spaced with intervals of five frames and centered at the nematode's center-of-mass, with head oriented to the right. Results reveal a distinct envelope of body postures specific to the motility environment.

are constructed using a principal component analysis to find the skeletons principal axis and orientation at each instant in time. Here, we may simply note that the near-symmetrical waveform seen during swimming in monodisperse medium [see Fig. 6(c)] is transformed into a somewhat more slithering-like motion as the nematode evolves in polydisperse medium [see Fig. 6(d)]; a motility trait that has been previously attributed to the differences in response and material properties between the two granular media [29]. Note that further quantitative locomotive phenotypes including the nematode wavelength and the amplitude of body undulations can be obtained in a seamless manner from the construction of such skeleton envelopes [17], [18], [20].

While our method provides a useable segmentation framework, some noticeable shortcomings are nevertheless apparent. In particular, we see that nematode skeletons are somewhat truncated in length and skeletons do not always sit along the centerline of the actual body. In general, the first shortcoming is a consequence of the difficult nature in accurately segmenting the head and tails of nematodes, as they are often transparent and are extremely similar to (or invisible against) the background environment. The second shortcoming results from both errors in the body segmentation (due to the complex background) and from the skeletonization process, which assumes that the correct centerline be equidistant from the boundaries of the segmented body.

Both of these shortcomings could be partly addressed by having a stronger model of the overall shape, head and tail of the nematode, as is the case in the work of Huang *et al.* [38]. Yet in general, the method outlined in [38] first relies on obtaining successful binary nematode segmentations to determine the correct body outline, from which a nematode skeleton is then extracted; in particular, this method has been solely applied to traditional crawling assays for the purpose of characterizing "foraging" behavior (i.e., rapid, side-to-side movement of the nematode head as it explores its environment). Since our method fails to segment the head and tail in a number of complex environments, integrating such strategies into our framework appears challenging when incorrect nematode contours and thus skeletons are generated.

Finally, we note an important limitation to our approach as a result of the static nature of the model. While we learn appropriate image features for given sequences, these are determined from the first image only in an effort to limit the user's manual labor and increase the easiness of the method. Yet, since some environments appear visually different as time lapses (i.e., as the sequence evolves), the models estimated from the initial image can become less accurate. This property is apparent in the discrepancies observed in the F-scores between the first image and the remaining sequence in a number of motility environments (see Table II). In turn, this greatly affects the quality of the produced final segmentations and potentially renders them unusable. In addition, we note that simply increasing the number of training images (i.e., using for instance the first ten images in an image sequence) to estimate the texture models does not appear to provide improved or more stable results (data not shown here). As such, our approach should not be expected to provide good nematode segmentations for scenarios where illumination of the fore- and/or background gradually changes across the sequence.

VI. Conclusion and Outlook

In this paper, we have proposed a novel TFM for automatic segmentation of nematode *C. elegans* in complex and dynamic visual environments. Our TFM method relies on the use of both intensity- and texture-based image features integrated within a probabilistic framework. This strategy first provides a coarse nematode segmentation from which we use an MRF model to refine our segmentation by inferring pixels belonging to the nematode by means of an approximate inference technique. To segment subsequent images in a sequence, we compute informative priors from the computed segmentations, via Bayesian filtering, and provide coherent estimates of nematode locations across time. We validate the TFM on a number of image sequences sampled across different visual environments and provide state-of-the-art results on challenging environments while assuring comparative performances to existing methods on traditional environments. In addition, we show how

C. elegans segmentations delivered with the TFM can be used to compute nematode skeletons from which motility phenotypes can then be extracted. This later point is extremely promising for high-throughput assays of motility phenotyping in complex environments.

In the future, we plan to extend our method to dynamically estimate image models as time proceeds in an effort to provide even better segmentations while improving strategies to segment the head and tail of nematodes more accurately. In addition, we will investigate methods for large-scale, automatic image feature learning that can adapt directly to specific environments and should provide overall improvements in nematode segmentations.

ACKNOWLEDGMENT

The authors would like to thank Dr. G. Juarez for helpful discussions.

REFERENCES

[1] S. Brenner, "The genetics of *Caenorhabditis elegans*," *Genetics*, vol. 77, pp. 71–94, 1974.

[2] J. E. Sulston and H. R. Horvitz, "Post-embryonic cell lineages of the nematode *Caenorhabditis elegans*," *Dev. Biol.*, vol. 56, pp. 110–156, 1977.

[3] J. E. Sulston, E. Schierenberg, J. G. White, and J. N. Thomson, "The embryonic cell lineage of the nematode *Caenorhabditis elegans*," *Dev. Biol.*, vol. 100, pp. 64–119, 1983.

[4] J. G. White, E. Southgate, J. N. Thomson, and S. Brenner, "The structure of the nervous system of the nematode *C. elegans*," *Phil. Trans. Roy. Soc. Lond. B Biol. Sci.*, vol. 314, pp. 1–340, 1986.

[5] C. E. S. Consortium, "Genome sequence of the nematode *C. elegans*: A platform for investigating biology," *Science*, vol. 282, pp. 2012–2018, 1998.

[6] A. Brown and W. Schafer, "Automated behavioural fingerprinting of *C. elegans* mutants," in in *Cambridge Series in Systems Genetics.*. Cambridge, U.K.: Cambridge Univ. Press, 2013.

[7] D. Ramot, B. E. Johnson, T. L. Berry, L. Carnell, and M. B. Goodman, "The parallel worm tracker: a platform for measuring average speed and drug-induced paralysis in nematodes," *PLOS One*, vol. 3, p. e2208, 2008.

[8] G. D. Tsibidis and N. Tavernarakis, "Nemo: A computational tool for analyzing nematode locomotion," *BMC Neuroscience*, vol. 8, 2007.

[9] S. D. Buckingham and D. B. Sattelle, "Fast, automated measurement of nematode swimming (thrashing) without morphometry," *BMC Neuroscience*, vol. 10, p. 84, 2009.

[10] C. J. Cronin, J. E. Mendel, S. Mukhtar, Y.-M. Kim, R. C. Stirb, J. Bruck, and P. W. Sternberg, "An automated system for measuring parameters of nematode sinusoidal movement," *BMC Genetics*, vol. 6, p. 5, 2005.

[11] J.-H. Baek, P. Cosman, Z. Feng, J. Silver, and W. R. Schafer, "Using machine vision to analyze and classify *Caenorhabditis elegans* behavioral phenotypes quantitatively," *J. Neurosci. Meth.*, vol. 118, no. 1, pp. 9–21, 2002.

[12] Z. Feng, C. J. Cronin, J. H. Wittig, P. W. Sternberg, and W. R. Schafer, "An imaging system for standardized quantitative analysis of *C. elegans* behavior," *BMC Bioinformatics*, vol. 5, p. 115, 2004.

[13] K.-M. Huang, P. Cosman, and W. R. Schafer, "Machine vision based detection of omega bends and reversals in *C. elegans*," *J. Neurosci. Meth.*, vol. 158, pp. 323–336, 2006.

[14] C. Fang-Yen, M. Wyart, J. Xie, R. Kawai, T. Kodger, S. Chen, Q. Wen, and A. Samuel, "Biomechanical analysis of gait adaptation in the nematode *Caenorhabditis elegans*," *Proc. Nat. Academy Sci. United States America*, vol. 107, pp. 20 323–20 328, 2010.

[15] S.-J. Park, M. B. Goodman, and B. L. Pruitt, "Analysis of nematode mechanics by piezoresistive displacement clamp," *Proc. Nat. Acad. Sci. USA*, vol. 104, pp. 17 376–17 381, 2007.

[16] B. Petzold, S.-J. Park, P. Ponce, C. Roozeboom, C. Powell, M. Goodman, and B. Pruitt, "*Caenorhabditis elegans* body mechanics are regulated by body wall muscle tone," *Biophysical J.*, vol. 100, pp. 1977–1985, 2011.

[17] J. Sznitman, P. K. Purohit, P. Krajacic, T. Lamitina, and P. E. Arratia, "Material properties of *Caenorhabditis elegans* swimming at low Reynolds number," *Biophysical J.*, vol. 98, pp. 617–626, 2010.

[18] J. Sznitman, X. Shen, P. K. Purohit, and P. E. Arratia, "The effects of fluid viscosity on the kinematics and material properties of *C. elegans* swimming at low Reynolds number," *Exp. Mech.*, vol. 50, pp. 1313–1311, 2010.

[19] J. Korta, D. A. Clark, C. V. Gabel, L. Mahadevan, and A. D. T. Samuel, "Mechanosensation and mechanical load modulate the locomotory gait of swimming *C. elegans*," *J. Exp. Biol.*, vol. 210, pp. 2383–2389, 2007.

[20] P. Krajacic, X. Shen, P. Purohit, P. Arratia, and T. Lamitina, "Biomechanical profiling of *Caenorhabditis elegans* motility," *Genetics*, vol. 191, pp. 1015–1021, 2012.

[21] J. Sznitman, X. Shen, R. Sznitman, and P. Arratia, "Propulsive force measurements and flow behavior of undulatory swimmers at low Reynolds number," *Phys. Fluids*, vol. 22, p. 121901, 2010.

[22] P. Sauvage, M. Argentina, J. Drappier, T. Senden, J. Siméon, and J. DiMeglio, "An elasto-hydrodynamical model of friction for the locomotion of *Caenorhabditis elegans*," *J. Biomechanics*, vol. 44, pp. 1117–1722, 2011.

[23] X. Shen, J. Sznitman, P. Krajacic, T. Lamitina, and P. Arratia, "Undulatory locomotion of *Caenorhabditis elegans* on wet surfaces," *Biophysical J.*, vol. 102, pp. 2772–2781, 2012.

[24] G. Stephens, B. Johnson-Kerner, W. Bialek, and W. Ryu, "Dimensionality and dynamics in the behavior of *C. elegans*," *PLOS Comput. Biol.*, vol. 4, p. e1000028, 2008.

[25] G. Stephens, L. Osborne, W. Bialek, "Searching for simplicity in the analysis of neurons and behavior," *Proc. Nat. Academy Sci. United States America*, vol. 108, pp. 15 565–15 571, 2011.

[26] A. Brown, E. Yemini, L. Grundy, T. Jucikas, and W. Schafer, "A dictionary of behavioral motifs reveals clusters of genes affecting *Caenorhabditis elegans* locomotion," *Proc. Nat. Academy Sci. United States America*, vol. 110, pp. 791–796, 2013.

[27] R. Ghosh and J. Sznitman, "Visualization of nematode *Caenorhabditis elegans* swimming in a liquid drop," *J. Visualization*, vol. 15, pp. 277–279, 2012.

[28] D. Albrecht and C. Bargmann, "High-content behavioral analysis of *Caenorhabditis elegans* in precise spatiotemporal chemical environments," *Nature Methods*, vol. 8, pp. 599–605, 2011.

[29] G. Juarez, K. Lu, J. Sznitman, and P. Arratia, "Motility of small nematodes in wet granular media," *Europhysics Lett.*, vol. 92, p. 44002, 2010.

[30] M. Mathew, N. Mathew, and P. Ebert, "Wormscan: A technique for high-throughput phenotypic analysis of *Caenorhabditis elegans*," *PLOS One*, vol. 7, p. e33483, 2012.

[31] N. Swierczek, A. Giles, C. Rankin, and R. Kerr, "High-throughput behavioral analysis in *C. elegans*," *Nature Methods*, vol. 8, pp. 592–598, 2011.

[32] J. Carr, A. Parashar, R. Gibson, A. Robertson, R. Martin, and S. Pandey, "A microfluidic platform for high-sensitivity, real-time drug screening on *C. elegans* and parasitic nematodes," *Lab Chip*, vol. 11, pp. 2385–2396, 2011.

[33] C. B. Rhode, F. Zeng, R. Gonzalesz-Rubio, M. Angel, and M. F. Yanik, "Microfluidic system for on-chip high-throughput whole-animal sorting and screening at subcellular resolution," *Proc. Nat. Acad. Sci. USA*, vol. 104, pp. 13 891–13 895, 2007.

[34] W. Shi, J. Qin, N. Ye, and B. Lin, "Droplet-based microfluidic system for individual *Caenorhabditis elegans* assay," *Lab Chip*, vol. 8, pp. 1432–1435, 2008.

[35] W. Geng, P. Cosman, J.-H. Baek, C. C. Berry, and W. R. Schafer, "Quantitative classification and natural clustering of *Caenorhabditis elegans* behavioral phenotypes," *Genetics*, vol. 165, no. 3, pp. 1117–1126, 2003.

[36] K. Hoshi and R. Shingai, "Computer-driven automatic identification of locomotion states in *Caenorhabditis elegans*," *J. Neuro. Meth.*, vol. 157, pp. 355–363, 2006.

[37] K.-M. Huang, P. Cosman, and W. R. Schafer, "Using articulated models for tracking multiple *C. elegans* in physical contact," *J. Sign. Process Syst.*, vol. 55, pp. 113–126, 2009.

[38] K. M. Huang, P. Cosman, and W. R. Schafer, "Automated detection and analysis of foraging behavior in *Caenorhabditis elegans*," *J. Neurosci. Meth.*, vol. 171, pp. 153–164, 2008.

[39] C. Stauffer and W. Grimson, "Adaptive background mixture models for real-time tracking," in *Proc. IEEE Conf. Comput. Vision Pattern Recog.*, 1999, pp. 246–252.

[40] R. Sznitman, M. Gupta, G. Hager, P. Arratia, and J. Sznitman, "Multi-environment model estimation for motility analysis of *Caenorhabditis elegans*," *PLOS One*, vol. 5, p. e11631, 2010.
[41] J. Karbowski, C. J. Cronin, A. Seah, J. E. Mendel, D. Cleary, and P. W. Sternberg, "Conservation rules, their breakdown, and optimality in *Caenorhabditis* sinusoidal locomotion," *J. Theor. Biol.*, vol. 242, pp. 652–669, 2006.
[42] J. T. Pierce-Shimomura, T. M. Morse, and S. R. Lockery, "The fundamental role of pirouettes in *Caenorhabditis elegans* chemotaxis," *J. Neurosci.*, vol. 19, pp. 9557–9569, 1999.
[43] J. T. Pierce-Shimomura, B. L. Chen, J. J. Mun, R. Ho, R. Sarkis, and S. L. McIntire, "Genetic analysis of crawling and swimming locomotory patterns in *C. elegans*," *Proc. Nat. Acad. Sci. USA*, vol. 105, pp. 20982–20987, 2008.
[44] N. Tavernarakis, W. Shreffler, S. Wang, and M. Driscoll, "unc-8, a DEG/ENAC family member, encodes a subunit of a candidate mechanically gated channel that modulates *C. elegans* locomotion," *Neuron.*, vol. 18, pp. 107–119, 1997.
[45] S. Berri, J. H. Boyle, M. Tassieri, I. A. Hope, and N. Cohen, "Forward locomotion of the nematode *C. elegans* is achieved through modulation of a single gait," *Human Frontier Sci. Program J.*, vol. 3, pp. 186–193, 2009.
[46] R. Ghosh and S. W. Emmons, "Episodic swimming behavior in the nematode *C. elegans*," *J. Exp. Biol.*, vol. 211, pp. 3703–3711, 2008.
[47] N. Chronis, M. Zimmer, and C. I. Bargmann, "Microfluidics for in vivo imaging of neuronal and behavioral activity in *Caenorhabditis elegans*," *Nature Methods*, vol. 4, pp. 727–731, 2007.
[48] A. Ghanbari, V. Nock, R. Blaikie, X. Chen, J. Chase, and W. Wang, "Automated vision-based force measurement of moving *C. elegans*," in *Proc. IEEE 6th Annu. Conf. Autom. Sci. Eng.*, 2010, pp. 198–203.
[49] S. Hulme, S. Shevkoplyas, J. Apfeld, W. Fontana, and G. Whitesides, "A microfabricated array of clamps for immobilizing and imaging *C. elegans*," *Lab Chip*, vol. 7, pp. 1515–1523, 2007.
[50] S. R. Lockery, K. J. Lawton, J. C. Doll, S. Faumont, S. M. Couthard, T. R. Thiele, N. Chronis, K. E. McCormick, M. B. Goodman, and B. L. Pruitt, "Artificial dirt: microfluidic substrates for nematode neurobiology," *J. Neurophysiol.*, vol. 99, pp. 3136–3143, 2008.
[51] S. Johari, V. Nock, M. Alkaisi, and W. Wang, "On-chip analysis of *C. elegans* muscular forces and locomotion patterns in microstructured environments," *Lab Chip*, vol. 13, pp. 1699–1707, 2013.
[52] T. Majmudar, E. Keaveny, J. Zhang, and M. Shelley, "Experiments and theory of undulatory locomotion in a simple structured medium," *J. Roy. Soc. Interface*, vol. 9, pp. 1809–1823, 2012.
[53] A. Parashar, R. Lycke, J. Carr, and S. Pandey, "Amplitude-modulated sinusoidal microchannels for observing adaptability in *C*. elegans locomotion," *Biomicrofluidics*, vol. 5, p. 024112, 2011.
[54] S. Park, H. Hwang, S.-W. Nam, F. Martinez, R. H. Austin, and W. S. Ryu, "Enhanced *Caenorhabditis elegans* locomotion in a structured microfluidic environment," *PLOS One*, vol. 3, p. e2550, 2008.
[55] J. Qin and A. R. Wheeler, "Maze exploration and learning in *C. elegans*," *Lab Chip*, vol. 7, pp. 186–192, 2007.
[56] S. Jung, "Caenorhabditis elegans swimming in a saturated particulate system," *Phys. Fluids*, vol. 22, p. 031903, 2010.
[57] J. Boyle, S. Johnson, and A. Dehghani-Sanij, "Adaptive undulatory locomotion of a *C. elegans* inspired robot," *IEEE/ASME Trans. Mechatronics*, vol. 18, no. 2, pp. 439–448, Apr. 2013.
[58] S. Kim, C. Laschi, and B. Trimmer, "Soft robotics: A bioinspired evolution in robotics," *Trends Biotechnol.*, vol. 31, pp. 287–294, 2013.
[59] H. Yuk, D. Kim, H. Lee, S. Jo, and J. Shin, "Shape memory alloy-based small crawling robots inspired by *C. elegans*," *Bioinspir. Biomim.*, vol. 6, p. 0460002, 2011.
[60] A. Lucchi, K. Smith, R. Achanta, G. Knott, and P. Fua, "Supervoxel-based segmentation of mitochondria in EM image stacks with learned shape features," *IEEE Trans. Med. Imag.*, vol. 31, no. 2, pp. 474–486, Feb. 2012.
[61] K. S. Camilus and V. K. Govindan, "A review on graph based segmentation," *Int. J. Image, Graphics Signal Process.*, vol. 4, no. 5, pp. 1–13, 2012.
[62] N. Roussel, C. A. Morton, F. P. Finger, and B. Roysam, "A computational model for *C. elegans* locomotory behavior: Application to multiworm tracking," *IEEE Trans. Biomed. Eng.*, vol. 54, no. 10, pp. 1786–1797, Oct. 2007.
[63] G. Tsechpenakis, L. Bianchi, D. N. Metaxas, and M. Driscoll, "A novel computational approach for simultaneous tracking and feature extraction of *C. elegans* populations in fluid environments," *IEEE Trans. Biomed. Eng.*, vol. 55, no. 5, pp. 1539–1549, May 2008.
[64] M. Piccardi, "Background subtraction techniques: A review," in *Proc. IEEE Int. Conf. Syst., Man Cybern.*, 2004, pp. 3099–3104.
[65] R. Sznitman, H. Lin, M. Gupta, and G. Hager, "Active background modeling: Actors on a stage," in *Proc. IEEE 12th Int. Conf. Comput. Vision, Workshop Vis. Surveillance*, 2009, pp. 1222–1228.
[66] K. Murphy, *Machine Learning: A Probabilistic Perspective*. Cambridge, MA, USA: MIT, 2012.
[67] T. Hastie, R. Tibshirani, and J. Friedman, *The Elements of Statistical Learning*. New York, NY, USA: Springer, 2001.
[68] J. Geusebroek, A. Smeulders, and J. van de Weijer, "Fast anisotropic Gauss filtering," *IEEE Trans. Image Process.*, vol. 12, no. 8, pp. 938–943, Aug. 2003.
[69] R. Sznitman, A. Lucchi, M. Cantoni, G. Knott, and P. Fua, "Flash scanning electron microscopy," presented at the Med. Image Comput. Comput.-Assist. Interv., Nagoya, Japan, Sep. 2013.
[70] S. Thrun, W. Burgard, and D. Fox, *Probabilistic Robotics*. Cambridge, MA, USA: MIT Press, 2005.
[71] A. Lucchi, K. Smith, R. Achanta, V. Lepetit, and P. Fua, "A fully automated approach to segmentation of irregularly shaped cellular structures in EM images," in *Proc. Med. Image Comput. Comput. Assist. Interv.*, 2010, pp. 463–471.

Ayala Greenblum received the B.Sc. degree in biomedical engineering from the Technion—Israel Institute of Technology, Haifa, Israel, in 2011, where she is currently working toward the M.Sc. degree in the Department of Biomedical Engineering, Biofluids Laboratory.

Her research interests include image processing, computer vision, and statistical learning for biomedical applications.

Raphael Sznitman received the B.Sc. degree in cognitive systems from the University of British Columbia, Vancouver, BC, Canada, in 2007, and the M.Sc. and Ph.D. degrees in computer science from Johns Hopkins University, Baltimore, MD, USA, in 2011.

He is currently a Postdoctoral Fellow at the Ecole Polytechnique Federale de Lausanne, Lausanne, Switzerland, where he works in the computer vision laboratory. His research interests include computational vision, probabilistic methods, and statistical learning, applied to applications in biomedical imaging.

Pascal Fua (F'12) received the Engineering degree from Ecole Polytechnique, Paris, France, in 1984, and the Ph.D. degree in computer science from the University of Orsay, Orsay, France, in 1989.

He joined Ecole Polytechnique Federale de Lausanne, the Swiss Federal Institute of Technology, Lausanne, Switzerland, in 1996, where he is currently a Professor in the School of Computer and Communication Science. Before that, he worked at SRI International and at INRIA Sophia-Antipolis as a Computer Scientist. His research interests include shape modeling and motion recovery from images, analysis of microscopy images, and augmented reality. He has (co)authored more than 200 publications in refereed journals and conferences.

Dr. Fua is an Associate Editor of the IEEE TRANSACTIONS FOR PATTERN ANALYSIS AND MACHINE INTELLIGENCE. He often serves as a Program Committee Member, Area Chair, and Program Chair of major vision conferences.

Paulo E. Arratia received the B.Sc. degree in chemical engineering from Hampton University, Hampton, VA, USA, in 1997, and the M.Sc. and Ph.D. degrees in chemical and biochemical engineering from Rutgers University, New Brunswick, NJ, USA, in 2001 and 2003, respectively.

He was a postdoctoral fellow at Haverford College (2003–2005) and the University of Pennsylvania (2005–2007). He is currently an Associate Professor in the Department of Mechanical Engineering and Applied Mechanics, University of Pennsylvania, Philadelphia, PA, USA. He is the Director of the Penn Complex Fluids Lab where his research interests focus on interdisciplinary soft-condensed matter and fluid dynamics, including swimming of microorganisms, blood flow in microfluidic devices, and viscoelasticity.

Josué Sznitman received the B.Sc. degree in mechanical engineering from the Massachusetts Institute of Technology, Cambridge, MA, USA, in 2002, and the Dipl.-Ing. and Dr. Sc. degrees in mechanical engineering from the ETH Zurich, Zurich, Switzerland, in 2003 and 2007, respectively.

Prior to joining the Department of Biomedical Engineering at the Technion—Israel Institute of Technology, Haifa, Israel, as an Assistant Professor in 2010, he was a Postdoctoral Researcher at the University of Pennsylvania (2008–2009) and a Lecturer and Research Associate at Princeton University appointed by the Council of Science and Technology. He is the founder of the Technion Biofluids Laboratory where his research interests include biofluid mechanics, quantitative flow visualization, and microfluidics.